Precise titanium isotope compositions of refractory inclusions in the Allende CV3 chondrite by LA-MC-ICPMS

C.D. Williams *, P.E. Janney [1], R.R. Hines, M. Wadhwa

Center for Meteorite Studies, School of Earth and Space Exploration, Arizona State University, Tempe, AZ 85287, United States

ARTICLE INFO

ABSTRACT

We present here analyses of mass-independent effects in the Ti isotope ratios of 17 coarse-grained (compact Type A and Type B) calcium–aluminum-rich inclusions (CAIs) from the Allende CV3 chondrite utilizing a method developed for rapid measurement of Ti isotopes by laser ablation multi-collector inductively coupled plasma mass spectrometry (LA-MC-ICPMS). Based on the analyses of the synthetic CMAS glasses doped with varying amounts of Ca, Cr and V, an empirical scheme for correction of potential isobaric interferences and matrix effects was developed. Using this scheme, mass-independent variations of the Ti isotope ratios $^{46}Ti/^{47}Ti$, $^{48}Ti/^{47}Ti$ and $^{50}Ti/^{47}Ti$ were measured with external reproducibilities (2SD) of ± 0.4, ± 0.5, and ± 1.8 for $\varepsilon^{46}Ti$, $\varepsilon^{48}Ti$, and $\varepsilon^{50}Ti$, respectively, based on repeat measurements of standard glasses. The Ti isotope compositions of the 17 Allende refractory inclusions analyzed here show that most of these CAIs are "normal" with limited variation in their mass-independent Ti isotope composition. One CAI (designated as CMS-1) has a significantly larger mass-independent $\varepsilon^{50}Ti$ anomaly and is identified as having Fractionation and Unidentified Nuclear (FUN) effects. The limited range in the Ti isotope compositions of normal CAIs ($\varepsilon^{50}Ti$ excesses ranging from 2.9 to 11.4) suggests that they originated from a nebular reservoir that was relatively well-mixed, although not completely homogenized (at the level of precision of the analyses reported here), in its isotopic composition. The distinctive isotopic composition of the FUN CAI CMS-1 indicates that it formed from a reservoir in the protoplanetary disk that was spatially or temporally distinct from that from which the normal CAIs were formed.

© 2016 Elsevier B.V. All rights reserved.

1. Introduction

Titanium has five stable isotopes, ^{46}Ti, ^{47}Ti, ^{48}Ti, ^{49}Ti and ^{50}Ti. The ratios of these isotopes, as measured in the components of carbonaceous chondrites, preserve information regarding nucleosynthetic sources of materials incorporated into the solar nebula, nebular processing, and the degree of isotopic heterogeneity in the early Solar System. Titanium isotopes were first employed as tracers of heterogeneity in the early Solar System over 30 years ago (Niederer et al., 1980, 1981, 1985; Niemeyer and Lugmair, 1981; Heydegger et al., 1982). These early studies reported resolvable Ti isotopic anomalies in meteorites, particularly associated with the neutron-rich isotope ^{50}Ti in calcium–aluminum-rich inclusions (CAIs) in carbonaceous chondrites. Subsequent studies have documented the presence of Ti isotopic anomalies in a wider range of meteoritic materials of Solar origin, but the largest effects are found in CAIs and their constituent minerals

(Niemeyer and Lugmair, 1984; Fahey et al., 1985, 1987; Ireland et al., 1985; Niederer et al., 1985; Zinner et al., 1986; Hinton et al., 1987; Papanastassiou and Brigham, 1989; Ireland, 1990; Leya et al., 2008, 2009; Chen et al., 2009; Trinquier et al., 2009).

CAIs are the oldest Solar System materials dated by absolute radiometric methods (Amelin et al., 2002, 2009; Jacobsen et al., 2008; Bouvier and Wadhwa, 2010; Bouvier et al., 2011; Connelly et al., 2011) and they preserve large isotopic anomalies for a range of elements. Previous Ti isotopic studies have focused primarily on Type A and Type B CAIs from CV chondrites (Niederer et al., 1980, 1981, 1985; Niemeyer and Lugmair, 1981; Heydegger et al., 1982; Papanastassiou and Brigham, 1989; Leya et al., 2009; Chen et al., 2009) as well as hibonite-bearing inclusions from CV and CM chondrites (Fahey et al., 1985, 1987; Ireland et al., 1985; Zinner et al., 1986; Hinton et al., 1987; Ireland, 1990). Hibonite-bearing inclusions and isolated hibonite grains exhibit the largest anomalies, as well as the widest overall range in Ti isotope compositions, with excesses in ^{50}Ti up to 98‰ (Fahey et al., 1985) and deficits as low as −69‰ (Hinton et al., 1987). The mass-independent Ti isotopic anomalies observed in hibonite-bearing inclusions display no correlation with their mass-dependent Mg isotope compositions. Therefore, it has been suggested that these isotopic anomalies represent a cosmochemical "memory" of nucleosynthetic anomalies originally hosted in interstellar dust (Clayton, 1978).

* Corresponding author at: Department of Earth and Planetary Sciences, University of California-Davis, Davis, CA 95616, United States.
    E-mail address: cdwill@ucdavis.edu (C.D. Williams).
[1] Now at Department of Geological Sciences, University of Cape Town, Private Bag X3, Rondebosch 7701 South Africa.

Investigation of the Ti isotopic compositions of Type A and Type B inclusions has been largely restricted to a select few CV chondrites (Allende, Leoville and Efremovka) and most of these (i.e., "normal" CAIs) display relatively small but resolvable excesses in ^{50}Ti (Niederer et al., 1980, 1981, 1985; Niemeyer and Lugmair, 1981; Heydegger et al., 1982; Papanastassiou and Brigham, 1989; Leya et al., 2009; Chen et al., 2009). Notable exceptions include so-called FUN CAIs, which display "Fractionated and Unidentified Nuclear effects" (FUN; Wasserburg et al., 1977). Two archetypical FUN CAIs are EK1-4-1 and C-1 (Niederer et al., 1980, 1981) from the Allende meteorite. When internally normalized to the ^{49}Ti/^{47}Ti ratio, the ^{50}Ti/^{47}Ti ratio of EK1-4-1 shows an excess of $\approx 15\varepsilon$ units, while C-1 exhibits a deficit of approximately 38ε units (ε units represent the deviation of a sample's Ti isotopic composition from terrestrial values in parts per 10^4). More recently, several more FUN CAIs have been identified that exhibit anomalies in ^{50}Ti that are comparable in magnitude to EK1-4-1 and C-1 (Papanastassiou and Brigham, 1989; Loss et al., 1994; Srinivasan et al., 2000). However, the limited dataset that currently exists makes it difficult to determine whether the measured range of Ti isotopic compositions in CAIs accurately reflects the degree of heterogeneity in the early Solar System or whether this heterogeneity may be considerably larger, but underestimated due to insufficient sampling and analysis of early Solar System materials. Therefore, a comprehensive Ti isotopic study of CAIs across several chondrite classes is needed to fully elucidate the degree of heterogeneity of Ti isotope compositions in CAIs. Toward this end, we have developed a method to rapidly determine the Ti isotopic composition of CAIs by LA-MC-ICPMS. This minimally destructive technique offers a precise and efficient means of determining the Ti isotopic compositions of a large suite of inclusions, allowing better constraints on the degree of isotopic heterogeneity in the Solar Nebula and the identification of additional FUN CAIs while preserving the bulk of the material for other detailed geochemical and isotopic investigations. Here, we report the Ti isotope compositions of 17 new Allende CAIs measured by LA-MC-ICPMS that provide further constraints on the degree of Ti isotope heterogeneity in the source reservoirs for these first solids formed in the Solar Nebula.

2. Methodology

Titanium isotope ratios were measured with a ThermoFinnigan Neptune multicollector inductively coupled plasma mass spectrometer (MC-ICPMS) in the Isotope Cosmochemistry and Geochronology Laboratory at Arizona State University (ASU). A Jet sample cone combined with a standard H-type skimmer cone was used in place of the standard H-sample and skimmer cone set, resulting in a five-fold increase in Ti sensitivity. Ultrapure water, aspirated through an APEX-Q sample introduction system, added a small amount of water vapor (approximately 20 μL/min volume equivalent) to the Ar makeup gas, which stabilized the ion beam signal and reduced interferences from

^{36}Ar^{12}C$^+$ and ^{36}Ar^{14}N$^+$ (Table 1). Isotope ratios were measured in multi-dynamic mode on Faraday cups in two peak jumping steps, measuring ^{44}Ca$^+$, ^{46}Ti$^+$, ^{47}Ti$^+$, ^{48}Ti$^+$, ^{49}Ti$^+$, ^{50}Ti$^+$ (in step 1) and ^{49}Ti$^+$, ^{51}V$^+$, ^{53}Cr$^+$ (in step 2) (Table 1). All analyses were made in medium resolution (m/Δm $\approx$ 5000) with integration times of 8.4 s in step 1 and 4.2 s in step 2. Each run consisted of 20 integrations, resulting in a five-minute analysis time. Gas blanks (same duration as sample analyses) were measured prior to acquisition of the first standard analysis in each analytical session and also immediately following each sample exchange.

In situ isotopic analyses of Ti-rich phases in polished mounts of Allende CAIs were performed using a Photon Machines Analyte 193 excimer laser ablation system connected to the MC-ICPMS, using He as carrier gas and Ar (with a small amount of added H$_2$O vapor) as makeup gas. See Janney et al. (2011) for details on the gas plumbing and conditions used for "moist plasma" analysis at ASU using the Analyte 193-Neptune system. All laser ablation measurements employed single spot analyses, using a 37 to 69 μm laser spot size (depending on the Ti abundance in the analyzed area) and 4 Hz repeat rate; laser power was 7 mJ/pulse (Table 2). Typical ^{48}Ti intensity during analyses of the standards (which have roughly 7 wt.% TiO$_2$) was 5–10 × 10^{-11} A. Instrumental and natural mass-dependent fractionation was corrected using the sample-standard bracketing technique and internal normalization to a ^{49}Ti/^{47}Ti ratio of 0.749766 (Niederer et al., 1981) using the exponential mass fractionation law,

$$R = r\left[1 + \frac{\Delta m}{m}\right]^{\beta} \tag{1}$$

where R is the true ratio, r is the measured isotopic ratio, $\Delta m/m$ is the relative mass difference of the Ti isotopes, and β represents the instrumental mass bias. Instrumental mass bass (β) corrections were calculated using

$$\beta = \frac{\ln\left[\frac{\left(\frac{^{49}Ti}{^{47}Ti}\right)_{True}}{\left(\frac{^{49}Ti}{^{47}Ti}\right)_{Measured}}\right]}{\ln\left[\frac{M_{49}}{M_{47}}\right]} \tag{2}$$

where (^{49}Ti/^{47}Ti)$_{True}$ is assumed to be 0.749766 (Niederer et al., 1981), M$_{47}$ and M$_{49}$ are the masses of ^{47}Ti and ^{49}Ti. The Ti isotopic compositions are expressed in the ε notation

$$\varepsilon^x Ti = \left[\frac{\left(\frac{^xTi}{^{47}Ti}\right)_{unknown}}{\left(\frac{^xTi}{^{47}Ti}\right)_{standard}} - 1\right] \cdot 10^4 \tag{3}$$

Table 1
Neptune cup configurations and possible interferences on Ti isotopes.

Cup configurations	L4	L3	L2	L1	Axial	H1	H2	H3	H4	Integ. time
Step 1	^{44}Ca$^+$	–	^{46}Ti$^+$	–	^{47}Ti$^+$	^{48}Ti$^+$	^{49}Ti$^+$	–	^{50}Ti$^+$	8.4 s
Step 2	–	^{49}Ti$^+$	–	^{51}V$^+$	–	^{53}Cr$^+$	–	–		4.2 s
Amplifier (Ohms)	10^{11}	10^{11}	10^{11}	10^{11}	10^{11}	10^{11}	10^{11}		10^{11}	
Potential interefences										
Mass	44	46	47	48	49	50	51	53		
Ti isotopic abund. (%)		8.25	7.44	73.72	5.41	5.18				
Singly-charged ions	^{44}Ca$^+$	^{46}Ca$^+$		^{48}Ca$^+$		^{50}V$^+$ ^{50}Cr$^+$	^{51}V$^+$	^{53}Cr$^+$		
Doubly-charged ions	^{88}Sr^{++}	^{92}Zr^{++} ^{92}Mo^{++}	^{94}Zr^{++} ^{94}Mo^{++}	^{96}Zr^{++} ^{96}Mo^{++}	^{98}Mo^{++}	^{100}Mo^{++}				
Polyatomic ions	^{28}Si^{16}O$^+$ ^{12}C^{16}O$_2^+$	^{14}N^{16}O$_2^+$	^{28}Si^{19}F$^+$	^{34}S^{14}N$^+$	^{35}Cl^{14}N$^+$ ^{34}S^{15}N$^+$	^{36}Ar^{14}N$^+$ ^{35}Cl^{15}N$^+$	^{36}Ar^{15}N$^+$ ^{35}Cl^{16}N$^+$	^{40}Ar^{13}C$^+$ ^{37}Cl^{16}O$^+$ ^{35}Cl^{18}O$^+$		

Table 2
Operating parameters for LA-MC-ICPMS system.

Laser ablation parameters		MC-ICPMS parameters	
Spot diameter used	37–69 μm	Cool gas flow rate	15 L/min
Repeat rate	4 Hz	Aux gas flow rate	1.0 L/min
Energy setting	100% (7 mJ)	Injector type	Quartz
Pulse length	4 ns	RF forward power	1200 W
Ablation cell dimensions	76 mm diam.	Extraction voltage	−2000 V
	5 mm height	Resolving power used	~5000
He ablation flow rate	~0.5 L/min	Accelerating voltage	10,000 V
Ar makeup gas flow rate	~0.5 L/min		
		APEX-Q parameters	
		Heated spray chamber temperature	125 °C
		Cooling coil temperature	2 °C
		Nebulizer uptake rate	200 μL/min
		Nitrogen flow	Off

where x = 46, 48 and 50. The internal statistics reported here for a single measurement of a sample is the arithmetic mean ($\overline{\chi}$) of individual blocks such that

$$\overline{\chi} = \frac{1}{N} \sum_{i=1}^{N} \chi_i \tag{4}$$

and twice its standard error (2SE) where

$$SE = SD/\sqrt{N}. \tag{5}$$

The external reproducibility, based on multiple analyses for each individual sample, is reported as twice its standard deviation (2SD) where

$$SD = \sqrt{\frac{1}{N-1} \sum (\chi_i - \overline{\chi})^2}. \tag{6}$$

Due to potentially large corrections required for isobaric interferences from Ca, V and Cr, and the fact that the assumption of identical mass bias values for Ti and the interfering element is not a robust one (i.e., $\beta_{Ca} \neq \beta_V \neq \beta_{Cr} \neq \beta_{Ti}$), we chose to use an empirical approach to correct our Ti isotope data for isobaric interferences. Synthetic glasses similar in composition to Ti–Al-rich pyroxene were prepared and doped with varying amounts of interfering species (Ca, V, Cr) expected to be encountered during the analysis of natural samples (Table 3). These glasses were analyzed in each analytical session and display linear correlations of measured deviations in the mass-independent Ti isotopic composition (e.g., ε^{50}Ti relative to the undoped glass) with the ratio of the abundance of interfering species to Ti (e.g., ^{53}Cr/^{49}Ti) (Fig. 1). Since these are synthetic glasses prepared from the same aliquots of Si, Al, Mg, Ti, Ca, V and Cr oxides, the mass-independent Ti isotopic compositions of the glasses are uniform and all measured variations in these compositions are attributable to isobaric interferences and potential matrix effects.

The Matlab Curve Fitting Toolbox Linear Least-Squares fitting method is applied to the uncorrected data to produce an equation in the form of

$$f(x) = p_1 x + p_2 \tag{7}$$

where is p_1 is the slope of the line, p_2 is the intercept and x is the ratio of the interfering specie to Ti (e.g., ^{53}Cr/^{49}Ti). The above equation is based on the uncorrected Ti isotope data obtained on the standard glasses (open black diamonds in Fig. 1) and is then applied to the data to obtain the corrected mass-independent Ti isotope ratio using the relationship of

$$\varepsilon^x Ti_{True} = \varepsilon^x Ti_{Measured} - f(x) \tag{8}$$

where $\varepsilon^x Ti_{Measured}$ is the measured value that has not been corrected for isobaric interferences and $\varepsilon^x Ti_{True}$ is the value after the correction has been applied (Fig. 1).

3. Samples

3.1. Synthetic fassaite glass standards

Matrix effects and isobaric interferences can cause analytical biases in the measured isotopic ratios during in situ analyses by LA-MC-ICPMS (see review by Shaheen et al., 2012). Therefore, well-characterized, isotopically homogeneous standards with elemental compositions similar to those of the samples are essential for accurate isotopic measurements. Synthetic glasses were prepared using Ca–Mg–Al–Si (CMAS) oxides that approximated the composition of Ti–Al-rich pyroxene (fassaite) commonly found in CAIs. Pure oxide powders were placed in a Pt-capsule, heated to high temperatures (>1500 °C) and then quenched in the *Depths of the Earth laboratory* (ASU). This glass was powdered, re-melted and quenched several more times to ensure homogeneity. Five fractions of this homogeneous glass were powdered and additionally doped with varying amounts of pure oxide powders of interfering species expected to be present during LA-MC-ICPMS analyses of refractory inclusions (i.e., Ca, Cr, V). These powders were then finally re-melted and quenched to produce glasses (Glasses #1–5 in Table 3). These glasses were mounted in an epoxy disk, which was then polished. One fraction of the undoped homogeneous glass was also mounted with the five doped glasses and was used as the bracketing standard ("Brack. Std." in Table 3) for measurement of the isotopic compositions of the synthetic doped glasses and natural samples. Major and minor element compositions of each of these glasses were measured on the CAMECA SX 100 electron microprobe at the University of Arizona; the homogeneity of these glasses was verified by multiple spot analyses on each glass. The compositions of these synthetic glasses are reported in Table 3.

3.2. Allende CAIs

We measured the Ti isotopic compositions of 17 coarse-grained CAIs (both compact Type A and Type B) from the Allende CV3 chondrite
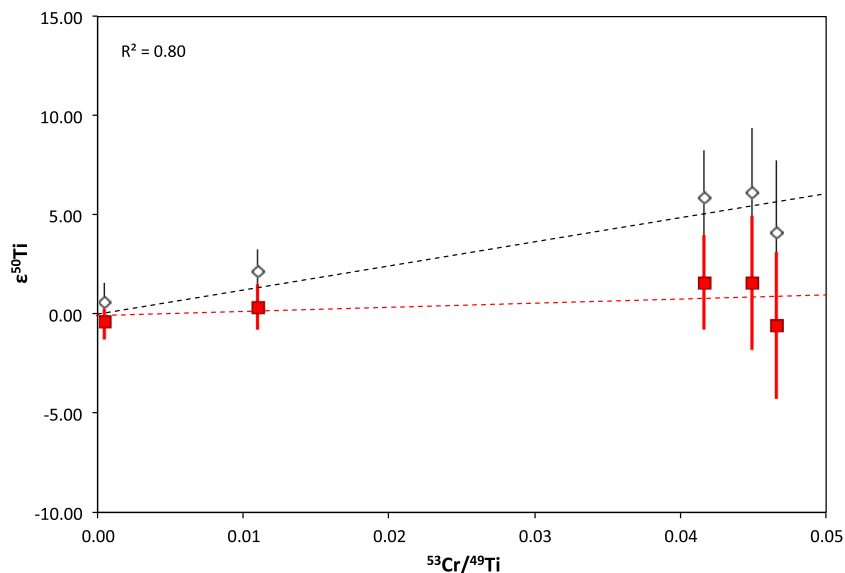
Table 3
Composition of synthetic CMAS glass standards measured by electron microprobe.

	Na$_2$O	MgO	Al$_2$O$_3$	K$_2$O	CaO	TiO$_2$	FeO	SiO$_2$	MnO	V	Cr	Total
	wt.%	wt.%	wt.%	wt.%	wt.%	wt.%	wt.%	wt.%	wt.%	ppm	ppm	wt.%
Brack. Std.	0.2	7.7	18.9	b.d.	25.9	7.2	0.5	39.6	b.d.	b.d.	b.d.	99.9
Glass #1	0.1	7.6	18.8	b.d.	26.6	7.1	0.5	39.3	b.d.	b.d.	b.d.	99.9
Glass #2	0.1	7.4	18.3	b.d.	27.3	6.9	0.9	38.3	b.d.	296	265	99.4
Glass #3	b.d.	7.6	18.8	b.d.	25.9	7.1	0.6	39.5	b.d.	b.d.	891	99.7
Glass #4	0.4	7.4	18.5	0.1	25.5	7.0	1.1	38.8	b.d.	2105	852	99.2
Glass #5	0.4	7.4	18.4	0.1	25.2	6.9	1.3	38.7	b.d.	4314	751	99.2

b.d. — below detection limit.

Fig. 1. Illustration of the empirical correction scheme for isobaric interferences from Cr on ^{50}Ti with uncorrected data obtained on the synthetic glass standards with varying Cr/Ti ratios represented by open black diamonds and the corrected data represented by solid red squares. These analyses were conducted during a single analytical session, where 4 repeat analyses were conducted on each of the five synthetic glasses; each data point is the average of these repeat analyses, shown here with the associated uncertainties (2SE). The R^2 value is 0.80 for the correlation line defined by the uncorrected data (black dashed line). The empirical correction (see text for details) is applied resulting in corrected data (solid red squares) that lie along the dashed red horizontal line within the errors. (For interpretation of the references to color in this figure legend, the reader is referred to the web version of this article.)

obtained from the collections at the Center for Meteorite Studies (CMS) at ASU and the Smithsonian Institution (SI) (Table 5). The samples investigated here included slabs, thick sections, and a small number of thin but unpolished slices of the Allende meteorite. The Ti-rich phases were identified using reconnaissance characterization of the samples by LA-MC-ICPMS, by monitoring the ^{48}Ti intensity during brief bursts of 10 laser pulses. If the ^{48}Ti intensity surpassed the critical threshold necessary for the acquisition of statistically robust analyses (typically 1×10^{-11} A beam intensity for ^{48}Ti), the position was recorded for analysis later in the session.

4. Results

4.1. Synthetic fassaite glass standards

Based on the analyses of the synthetic CMAS glasses doped with varying amounts of Ca, Cr and V, an empirical scheme for correction of potential isobaric interferences and matrix effects was developed. Using this scheme, the external reproducibilities (2SD) for ε^{46}Ti, ε^{48}Ti, and ε^{50}Ti (based on repeated analyses of the synthetic glasses) are ± 0.4, ± 0.5, and ± 1.8, respectively (Table 4, Fig. 2a,b,c). This precision is an order of magnitude better than that obtained by SIMS investigations (Fahey et al., 1985, 1987; Hinton et al., 1987; Ireland, 1990; Ireland et al., 1985; Zinner et al., 1986), and several times more precise than that reported by previous TIMS studies (Niederer et al., 1980, 1981, 1985; Niemeyer and Lugmair, 1981, 1984; Heydegger et al., 1982; Papanastassiou and Brigham, 1989) or another recent LA-MC-ICPMS

study (Chen et al., 2009). However, recent Ti isotope analyses by solution-based MC-ICPMS (e.g., Zhang et al., 2011, 2012) display increased precision since these measurements are typically run at high concentrations (resulting in high Ti beam intensities) of purified Ti sample solutions with limited contributions from interfering species.

4.2. Allende CAIs

We have measured the Ti isotopic compositions of 17 Allende CAIs. Table 5 reports the average Ti isotope composition (along with the associated 2SD uncertainty) for each CAI based on multiple spot analyses (with number of analyses, n, ranging from 2 to 10) on each inclusion. We did not observe any intra-inclusion variation in the Ti isotope composition outside of the analytical uncertainty for any given CAI. Given this, as well as the fact the analyses were made on the Ti-rich phases (that dominate the Ti inventory of each inclusion), we believe that the average Ti isotope composition reported in Table 5 for each CAI based on multiple spot analyses is representative (at least at the level of precision of this current study) of the bulk Ti isotope composition of that CAI. In this context, it is also noteworthy that no intra-inclusion variability in mass-independent Ti isotope compositions has been reported by previous in situ investigations of any refractory inclusions (e.g., Fahey et al., 1987; Ireland, 1990; Chen et al., 2009).

With the notable exception of inclusion CMS-1, the compositions of nearly all other compact Type A and Type B Allende inclusions analyzed here are similar within uncertainties (Table 5). The population of CAIs, on average, displays resolved excesses in ^{50}Ti relative to the terrestrial standard composition (Fig. 3a); these isotopic compositions are also in agreement with those previously reported for "normal" Type A and Type B inclusions from Allende (Niederer et al., 1980, 1981, 1985; Niemeyer and Lugmair, 1981; Heydegger et al., 1982; Papanastassiou and Brigham, 1989; Leya et al., 2009; Chen et al., 2009; Zhang et al., 2011). As such, our findings so far suggest that "normal" Type A and Type B CAIs formed from a relatively well-mixed isotopic reservoir in the Solar Nebula, but this remains to be tested with additional analyses of CAIs from a broader suite of primitive chondrites.

Inclusion CMS-1 has a Ti isotopic composition that is clearly distinct from that of other CAIs that we have analyzed so far (Table 5; Fig. 3b). CMS-1 is a relatively large (~5 mm in the longest dimension),
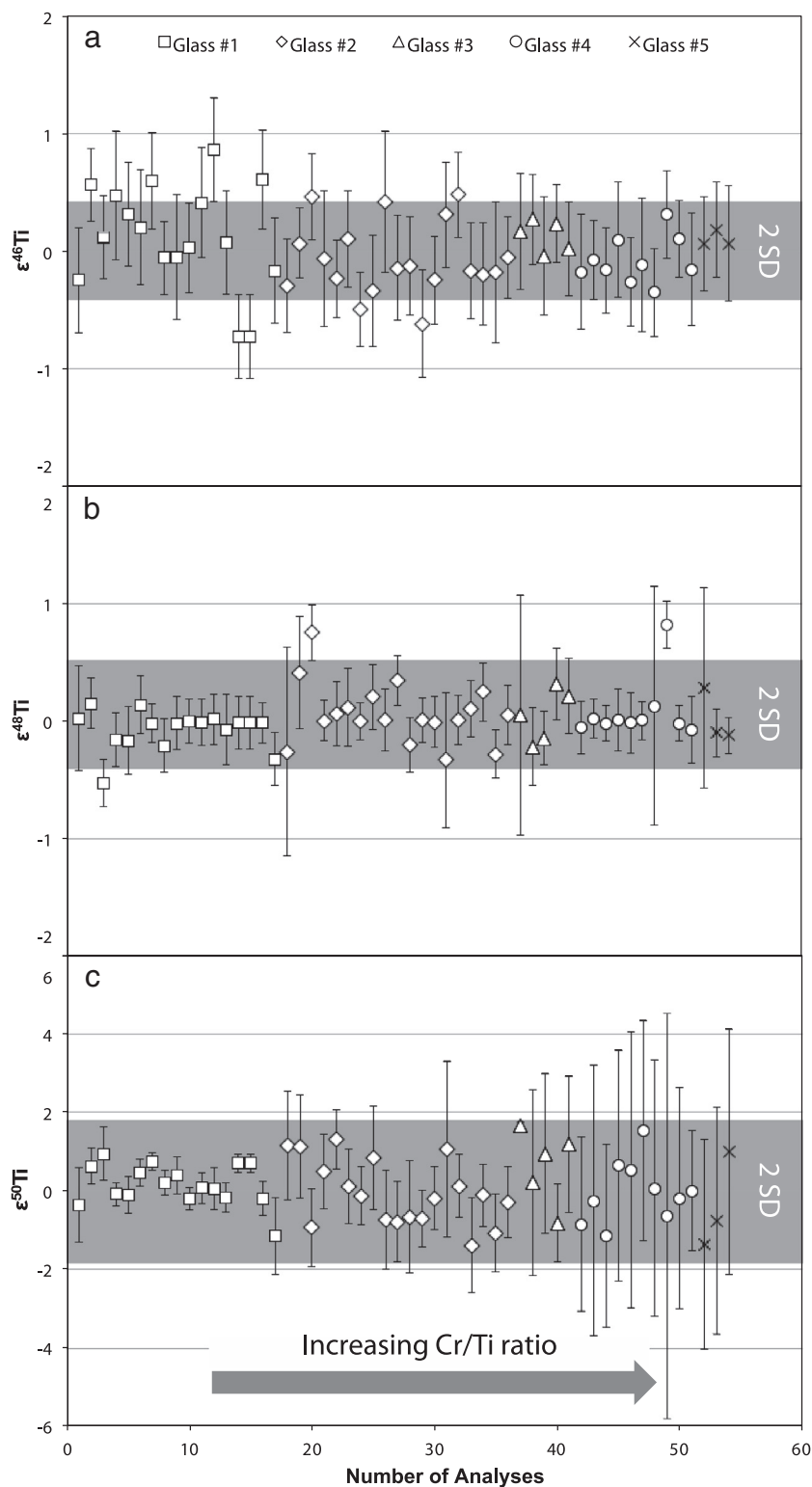
Table 4
Titanium isotopic composition of CMAS glass standards measured in situ by LA-MC-ICPMS.

Name	n	ε^{46}Ti	2SD	ε^{48}Ti	2SD	ε^{50}Ti	2SD
Glass #1	17	0.1	0.9	−0.1	0.3	0.2	1.1
Glass #2	19	−0.1	0.6	0.1	0.5	0.0	1.7
Glass #3	5	0.1	0.3	0.0	0.5	0.6	1.9
Glass #4	10	−0.1	0.4	0.1	0.5	0.0	1.6
Glass #5	3	0.1	0.1	0.0	0.5	−0.4	2.4

Mean values for repeat measurements and external 2SD uncertainties.

Fig. 2. Empirically corrected Ti isotope data for the doped fassaite glasses. The long-term, external reproducibilities (2SD) are shown as the gray shaded regions; these are calculated as twice the standard deviation based on multiple repeat analyses and are (a) ±0.4 for ε^{46}Ti, (b) ±0.5 for ε^{48}Ti, and, and (c) ±1.8 for ε^{50}Ti, respectively. Error bars shown for individual data points are 2SE internal errors.

irregularly shaped inclusion whose Ti isotopic composition is ε^{46}Ti = −13.9 ± 1.7, ε^{48}Ti = 0.2 ± 0.7, ε^{50}Ti = −51.3 ± 6.9. The deficits in ^{46}Ti and ^{50}Ti are well outside the range of Ti isotopic compositions observed for "normal" CAIs, but similar to those reported

previously in other FUN CAIs (Papanastassiou and Brigham, 1989; Loss et al., 1994; Niederer et al., 1980, 1981, 1985). Large mass-dependent fractionation in the Mg, Si and O isotopic compositions of CMS-1 confirms its classification as a FUN CAI (Williams et al., 2012, 2013).

Table 5
Titanium isotopic composition of Allende CAIs measured in situ by LA-MC-ICPMS.

Sample	Collection	n	$\varepsilon^{46}Ti^{(b)}$	2SD	$\varepsilon^{48}Ti^{(b)}$	2SD	$\varepsilon^{50}Ti^{(b)}$	2SD
CAI 8A33	SI	5	1.1	1.5	1.3	0.7	9.0	2.9
CAI 9A30	SI	10	3.1	0.9	0.2	0.5	8.3	3.3
CAI 3B75	SI	4	3.1	1.6	1.1	0.7	9.0	1.3
CAI A3-6large	CMS	2	1.8	2.3	0.7	1.7	9.1	2.5
CAI B7-A-big	CMS	7	0.8	1.8	1.2	1.2	7.9	2.0
CAI B7-A-little	CMS	8	−0.7	0.9	1.1	1.4	6.9	3.8
CAI B7-B-big	CMS	5	0.3	2.0	0.7	1.0	8.8	0.7
CAI B7-N	CMS	8	−1.3	2.0	1.4	0.7	7.9	3.7
CAI B7-S-B2	CMS	6	4.0	0.7	0.1	0.1	16.4	2.2
CAI B7-Ssub2-B1	CMS	5	1.8	1.2	0.0	0.0	3.7	4.2
CAI B1	CMS	5	−3.7	0.4	0.1	0.1	2.9	1.9
CAI B2	CMS	7	−1.9	1.7	0.1	0.0	10.1	4.3
CAI G3	CMS	8	2.5	1.2	−0.8	1.1	8.5	2.0
CAI G2	CMS	5	0.7	1.4	1.6	0.9	8.6	3.4
CAI W-2	CMS	2	1.9	0.8	−0.2	1.6	7.3	0.8
CAI W-W	CMS	5	0.4	3.0	−0.1	2.6	11.4	2.6
CAI CMS-1	CMS	8	−13.9	1.7	0.2	0.7	−51.3	6.9

Mean values for repeat measurements and external 2SD uncertainties.

5. Discussion

5.1. Sampling statistics

Given the limited existing database on the Ti isotopic composition of CAIs, underlying biases due to sampling statistics may have hindered previous interpretations regarding isotopic heterogeneity in the early Solar System. For example, with the limited number of analyses (of both "normal" and FUN CAIs) obtained to date, it is still unclear whether the available CAI Ti isotope data indicate that there is a single population of CAIs (i.e., formed at the same time from a spatially limited reservoir) with a large spread in their Ti isotopic compositions or whether there are multiple isotopically homogeneous sub-populations (i.e., that formed in distinct spatial and/or temporal regimes in the protoplanetary disk). In the following, we have taken into consideration the Ti isotopic data for CAIs obtained in the past and discuss, in the context of the new data presented here, how future LA-MC-ICPMS analyses can assist in overcoming sampling bias in the database.

Based on their isotopic compositions obtained thus far, CAIs may be divided into two subsets: 1) the more common "normal" CAIs, which display relatively limited isotopic variation, and 2) the rarer FUN CAIs that display large excesses or deficits in their Ti isotopic compositions (as well as mass-dependent isotopic fractionations) that fall well outside the isotopic range observed in "normal" CAIs. Based on all the Ti isotope data available thus far, identification of FUN CAIs can be accomplished by subjecting the data to an outlier rejection scheme. For example, by compiling previously published data on both "normal" and FUN CAIs from Allende, we can compute the arithmetic mean and twice the standard deviation (2SD) (the arithmetic mean and its associated standard deviation are used here since we were unable to accurately propagate errors when converting some of the literature data to the $^{49}Ti/^{47}Ti$ normalization scheme used in this study). Using these calculations, any CAI analysis that falls outside the 2SD limits can be characterized as FUN and the dataset iterated through again until no outliers remain. When complete, this procedure divides the current dataset into multiple subsets, with the vast majority of inclusions characterized by relatively limited Ti isotopic compositions ($\varepsilon^{46}Ti = 1.1 \pm 3.4$, $\varepsilon^{48}Ti = 0.9 \pm 3.8$, $\varepsilon^{50}Ti = 9.5 \pm 6.0$; n = 49) which we refer to as "normal" CAIs. The FUN CAIs fall well outside of this range of Ti isotope compositions. However, this method of characterizing populations of CAIs is only valid if the populations have been adequately sampled.

The number of analyses required for a given level of confidence in the characterization of population can be estimated (Dodson et al., 1988). Following the example laid out by Dodson et al. (1988), let us consider the probability that an isotopically distinct population of CAIs might have been missed during the sampling of Allende inclusions. If *f*
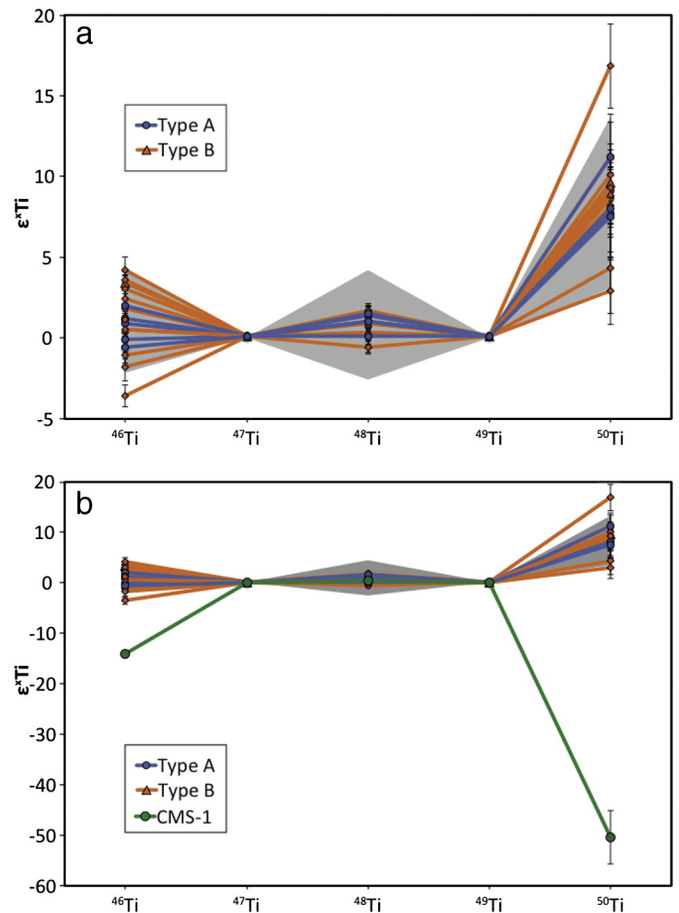

Fig. 3. (a) Mass-bias normalized Ti isotopic composition of compact Type A and Type B Allende CAIs. Shaded region shows the range of Ti isotopic compositions in "normal" CAIs (Niederer et al., 1980, 1981, 1985; Niemeyer and Lugmair, 1981; Heydegger et al., 1982; Papanastassiou and Brigham, 1989; Leya et al., 2009; Chen et al., 2009). Colored symbols are from this study. (b) Titanium isotopic composition of compact Type A and Type B Allende CAIs as well as that of CMS-1 (green circle). Error bars are 2SD external errors based on multiple repeat analyses. (For interpretation of the references to color in this figure legend, the reader is referred to the web version of this article.)

(a value between 0 and 1) is the frequency (i.e., rate of occurrence) of such an isotopically distinct population, the probability *P* of completely missing a population when selecting *n* number of inclusions at random can be expressed as

$$P = [1-f]^n \tag{9}$$

If we set n equal to the total number of CAIs for which Ti isotope compositions have been reported in the literature (i.e., n = 32; Niederer et al., 1980, 1981, 1985; Niemeyer and Lugmair, 1981; Heydegger et al., 1982; Papanastassiou and Brigham, 1989; Leya et al., 2009; Chen et al., 2009), we find that there is an even chance (P ~0.5) of having missed a hypothetical population with a distinct isotopic composition with a frequency of 0.02 (i.e., having missed a hypothetical population of distinct isotopic composition whose abundance comprises 2% of all natural samples). However, there is only a ~5% chance of having missed a population with a frequency of 0.09. In other words, given a distinct population making up 9% of all natural samples, there is less than 1 chance in 20 that the analyses made previously would have missed this population. If we add the 17 analyses from this study to the existing data (n = 49), the probability of having missed a population of isotopically distinct inclusions is only ~5% if their abundance is greater than 6% and 3 in 100 if another 30 inclusions are analyzed (for f = 0.037). However, the majority of analyses performed to date have been restricted to a few CV chondrites (primarily Allende,
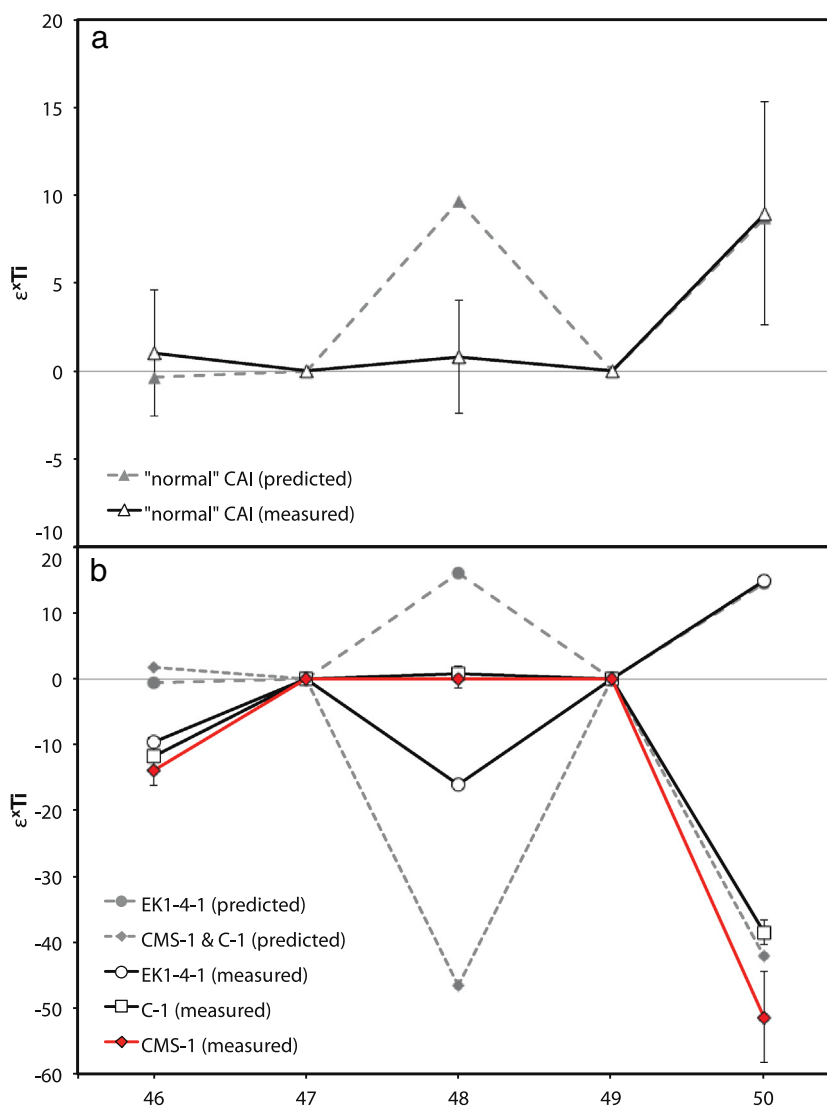
Fig. 4. The measured mass-independent anomalies in Ti isotopes compared with predicted ones for (a) "normal" CAIs and (b) FUN CAIs. (a) The average Ti isotopic composition of "normal" CAIs (from this study; Niederer et al., 1980, 1981, 1985; Niemeyer and Lugmair, 1981; Heydegger et al., 1982; Papanastassiou and Brigham, 1989; Leya et al., 2009; Chen et al., 2009) is plotted as open triangles. The nuclear field shift effect calculated to match the anomaly in ε^{50}Ti is represented by the gray filled triangles and dashed line. The best fit to the ε^{50}Ti value occurs when $a = 180$. (b) The Ti isotopic composition of Allende FUN CAIs (Niederer et al., 1980, 1981, 1985) is plotted as open circles (EK1-4-1), open squares (C-1), and red diamonds (CMS-1). The calculated nuclear field shift effect is shown as the gray filled symbols and dashed lines. The best fit to the ε^{50}Ti value for EK1-4-1 on one hand, and the average ε^{50}Ti value for C-1 and CMS-1 on the other, occurs when $a = 300$ and -870, respectively. Error bars shown for the "normal" and FUN CAI data are 2SD. (For interpretation of the references to color in this figure legend, the reader is referred to the web version of this article.)

Leoville and Efremovka). This sampling bias decreases our confidence with regards to having accurately identified all distinct Ti isotopic populations that comprise Type A and B CAIs (see discussions by Anderson, 2005 and Vermeesch, 2004). The rapid acquisition of Ti isotopic composition data presented here, requiring minimal sample preparation and destruction, applied to CAIs in a wider range of primitive chondrite types, would provide the opportunity to significantly increase our confidence in the characterization of isotopically distinct populations among these earliest-formed Solar System solids (and, of the degree of isotopic heterogeneity in the Solar Nebula).

5.2. Nuclear field shift versus nucleosynthetic effects

Previous studies have demonstrated that the Ti isotopic composition of Type A and B CAIs deviate significantly from terrestrial values (Niederer et al., 1980, 1981, 1985; Niemeyer and Lugmair, 1981; Heydegger et al., 1982; Papanastassiou and Brigham, 1989; Leya et al., 2009; Chen et al., 2009). These studies have attempted to use the Ti

isotopic composition of CAIs to identify nucleosynthetic components and describe the relative efficiency of mixing in the early Solar System. However, it should also be noted that mass-independent fractionation of Ti isotopes has been observed in chemical exchange experiments and theoretical nuclear field shift effects have successfully reproduced the magnitude, and direction, of these observed isotopic fractionations (Fujii et al., 1998). These experiments prompted Fujii et al. (2006) to extend these predictions to the isotopic compositions of FUN CAIs. Here, we briefly review nuclear field shift effects and show that the Ti isotopic anomalies observed in both "normal" and FUN CAIs are not plausibly explained by nuclear fields shift effects and, rather, must reflect incomplete mixing of distinct nucleosynthetic sources in the early Solar System.

Mass-independent isotope fractionation by the nuclear field shift is caused by the preferential partitioning of isotopes in chemical reactions because of differences in the size, shape and charge between nuclei. These isotopic fractionations can be predicted based on differences in the mean-squared nuclear charge radii between isotopes (Bigeleisen,

1996). Mass-independent isotope effects are calculated using the following equation (Fujii et al., 2006):

$$\varepsilon_{mi} = \left[\delta\langle r^2 \rangle_{m1,mi} - \frac{m2(mi-m1)}{mi(m2-m1)} \cdot \delta\langle r^2 \rangle_{m1,m2} \right] \cdot a \tag{10}$$

where m1 and m2 are the atomic masses of the nuclides chosen for internal normalization, and mi represents the atomic mass of a nuclide indexed with the variable "i." Differences in mean-squared nuclear charge radii, $\delta\langle r^2 \rangle$, of each isotope pair are taken from Angeli (2004). Differences in mean-squared nuclear charge radii, along with the measured ε_{mi} values of the samples, are combined into the equation above, leaving the parameter "a" to be determined by regression. The variable "a" is an adjustable parameter depending on temperature and represents the overall extent of mass-independent isotope fractionation (Fujii et al., 2006).

The Ti isotopic compositions of "normal" and FUN CAIs are shown in Fig. 4a,b along with the predicted nuclear field shift effects calculated to match the $\varepsilon^{50}Ti$ values for these CAIs. As can be seen, these effects can successfully reproduce the excess observed in ^{50}Ti for "normal" CAIs when the parameter "a" is equal to 180 (Fig. 4a). However, the theory of nuclear field shift effects predicts that excesses in ^{50}Ti should be accompanied by excesses in ^{48}Ti as well, which is not observed. Nuclear field shift is also incapable of producing the deficits in ^{46}Ti that are observed in FUN CAIs (Fig. 4b). Regardless of how "a" values are optimized, discrepancies still exist between the observed isotopic anomalies in ^{48}Ti and ^{50}Ti for FUN CAIs and those predicted by nuclear field shift effects (Fujii et al., 2006). This suggests that this type of mass-independent fractionation process played only a minor role, if any, in determining the Ti isotopic composition of early Solar System materials.

5.3. Mixing of distinct nucleosynthetic sources and late injection of supernova material

In discussing the patterns of Ti isotope anomalies it is convenient to consider constraints provided by multi-component mixing models. If we consider the systematics of multicomponent mixing for i isotopes and k distinct components, we can write

$$\left(\frac{{}^{i}Ti}{{}^{47}Ti} \right)_{mix} = \frac{\sum \left(\frac{{}^{i}Ti}{{}^{47}Ti} \right)_k \cdot f_k \cdot [Ti]_k}{\sum f_k \cdot [Ti]_k} \tag{11}$$

where $({}^{i}Ti/{}^{47}Ti)_k$ is the Ti isotope ratio of component k in the mixture; f_k is the fraction in the mixture of the contributed component and $[Ti]_k$ is the concentration of Ti contributed by component k to the mixture. In practice, the problems of interest are the determination of the minimum number of distinct components required to obtain the observed isotopic compositions, and the determination of the ratios $({}^{i}Ti/{}^{47}Ti)_k$ for the components.

To establish the minimum number of components required to describe the observed variance in the Ti isotope compositions reported thus far for Allende CAIs (including the data obtained in this study), we consider the three dimensional representation for $^{46}Ti/^{47}Ti$, $^{48}Ti/^{47}Ti$ and $^{50}Ti/^{47}Ti$, which are the three independent ratios after normalization of the data for mass-dependent fractionation effects. Using principal component analysis (PCA), which is a mathematical method for assessing variable groupings within multivariate data, we can establish the minimum number of components needed to account for the total variance observed in the Ti isotopic data of "normal" CAIs. The ^{46}Ti and ^{50}Ti signatures expressed in the data of "normal" CAIs dominate the variance described by these components. Heydegger et al. (1982); Niederer et al. (1981, 1985) and Niemeyer and Lugmair (1981, 1984) have previously shown that at least three distinct endmember components are required to explain the Ti isotopic variability in "normal" CAIs from the Allende meteorite. These studies also suggested that a fourth component might be necessary to explain the Ti isotopic

variability in Allende CAIs if FUN CAIs are included. Incorporating FUN CAIs into a dataset with "normal" CAIs, when attempting to calculate the number of components necessary to explain the variance in the CAI source reservoir in the Solar Nebula at any given time, is valid if these inclusions formed coevally. However, if "normal" CAIs and FUN CAIs originated during temporally distinct episodes, then such calculations are not strictly valid since the degree of mixing of the presolar components with distinct compositions likely evolved with time. Nevertheless, FUN CAIs may represent endmember components (or lie along vectors toward endmember components) that subsequently mixed to produce the observed Ti isotopic compositions in "normal" CAIs.

"Normal" CAIs from this study and others (Niederer et al., 1980, 1981, 1985; Niemeyer and Lugmair, 1981, 1984; Heydegger et al., 1982; Papanastassiou and Brigham, 1989; Leya et al., 2009; Chen et al., 2009) display positive excesses in both $\varepsilon^{46}Ti$ and $\varepsilon^{50}Ti$. Preliminary high-precision Ti isotope data obtained via solution MC-ICPMS for several Allende CAIs (Davis et al., 2016) also suggest a high degree of correlation between $\varepsilon^{46}Ti$ and $\varepsilon^{50}Ti$. This association is interesting when considering ^{46}Ti is likely the product of a neutron-poor stellar source region while ^{50}Ti is likely the product of a neutron-rich stellar source region. The observed trend requires the products of at least two distinct stellar sources being present in the region of "normal" CAI formation. Several potential scenarios exist to explain this correlation including mixing of multiple components, one of which has ^{46}Ti inherited from the H zone of Type II supernova (SN II) and another has ^{50}Ti inherited from a Type Ia supernova (SN Ia) (Rauscher et al., 2002; Woosley, 1997). Yet, the source of the ^{50}Ti excesses observed in "normal" CAIs is still unknown. The primary producer of ^{50}Ti, and most other neutron-rich iron-group isotopes, is predicted to be associated with Type Ia supernovae (Woosley, 1997). However, the production of ^{50}Ti has also been predicted via the slow neutron capture process (s-process) in asymptotic giant branch (AGB) stars (Lugaro et al., 2004). As such, Ti isotope compositions cannot, by themselves, distinguish between these two stellar sources. Complementary ^{48}Ca isotope measurements might provide additional insight into which stellar source is responsible for the ^{50}Ti excesses since theoretical work suggests that ^{48}Ca cannot be ejected in significant quantities from AGB stars (Woosley, 1997). There have been several reports of ^{48}Ca excesses observed in CAIs (Chen et al., 2015; Huang et al., 2011; Jungck et al., 1984; Lee et al., 1978, 1979; Loss et al., 1994; Niederer and Papanastassiou, 1984; Papanastassiou and Brigham, 1989; Russell et al., 1998; Moynier et al., 2010; Weber et al., 1995). However, strong, linear correlations with ^{50}Ti are not always observed. Further high-precision isotopic measurements of a well-characterized suite of CAIs are necessary before more definitive conclusions regarding distinct stellar sources can be drawn.

Both FUN and "normal" CAIs are characterized by Ti isotopic compositions that are distinct from terrestrial values. "Normal" CAIs exhibit relatively limited variation in their Ti isotopic compositions, and are characterized by mass-independent excesses in ^{50}Ti. The Ti isotopic compositions of "normal" CAIs require at least three distinct components (as discussed above) that were relatively well-mixed on their timescale of formation given their limited Ti isotopic variability. This suggests that the "normal' CAI source reservoir in early Solar Nebula likely experienced one or more discrete heating events that homogenized the Ti isotopic composition in this reservoir and resulted in the formation of "normal" Type A and B CAIs such as those analyzed here. However, as noted previously, the Ti isotopic compositions (particularly, $\varepsilon^{50}Ti$) of "normal" CAIs are clearly distinct from terrestrial values. This difference may be the result of radial variations in the Ti isotope composition, as discussed by Leya et al. (2008) and Trinquier et al. (2009), or it may suggest late-stage injection or admixing of neutron-poor Ti isotopic material between the time of "normal" CAI formation and accretion of the Earth. Deficits in $\varepsilon^{50}Ti$ have been reported for several FUN CAIs including CMS-1 (this study), which may indicate late

addition of supernova material into the Solar System or vaporization and mixing of a pre-existing supernova component after the formation of these FUN CAIs but prior to planet formation.

6. Summary

A new method is presented here for the measurement of Ti isotope compositions by LA-MC-ICPMS using a Photon Machines Analyte 193 excimer laser ablation system connected to a ThermoFinnigan Neptune MC-ICPMS. An empirical scheme for correction of potential isobaric interferences and matrix effects was developed based on analysis of synthetic CMAS glasses doped with varying amounts of Ca, Cr and V. The external reproducibilities (2SD) for $\varepsilon^{46}Ti$, $\varepsilon^{48}Ti$, and $\varepsilon^{50}Ti$ using this scheme are ± 0.4, ± 0.5, and ± 1.8, respectively. The Ti isotopic compositions of 17 Allende CAIs are reported including one newly identified FUN CAI. The Ti isotopic compositions of "normal" CAIs reported here define a narrow range with clearly resolved excesses in ^{46}Ti and ^{50}Ti. These findings suggest that "normal" CAIs formed from a relatively well-mixed reservoir. This reservoir was spatially or temporally distinct from that in which FUN CAIs originated.

Acknowledgments

Appendix A. Supplementary data

Supplementary data to this article can be found online at http://dx.doi.org/10.1016/j.chemgeo.2016.04.021.

References

Amelin, Y., Krot, A.N., Hutcheon, I.D., Ulyanov, A.A., 2002. Lead isotopic ages of chondrules and calcium–aluminum-rich inclusions. Science 297, 1678–1683.

Amelin, Y., Connelly, J., Zartman, R.E., Chen, J.H., Gopel, C., Neymark, L.A., 2009. Modern U–Pb chronometry of meteorites: advancing to higher time resolution reveals new problems. Geochim. Cosmochim. Acta 73, 5212–5223.

Anderson, T., 2005. Detrital zircons as tracers of sedimentary provenance: limiting conditions from statistics and numerical simulation. Chem. Geol. 216, 249–270.

Angeli, I., 2004. A consistent set of nuclear rms charge radii: properties of the radius surface R(N,Z). At. Data Nucl. Data Tables 87, 185–206.

Bigeleisen, J., 1996. Nuclear size and shape effects in chemical reactions; isotope chemistry of the heavy elements. J. Am. Chem. Soc. 118, 3676–3680.

Bouvier, A., Wadhwa, M., 2010. The age of the solar system redefined by the oldest Pb–Pb age of a meteoritic inclusion. Nat. Geosci. 3, 637–641.

Bouvier, A., Brennecka, G.A., Wadhwa, M., 2011. Absolute chronology of the first solids in the solar system. Workshop on Formation of the First Solids in the Solar System, #9054.

Chen, H.-W., Lee, T., Lee, D.-C., Iizuka, Y., 2009. In situ Ti isotopic measurements by laser ablation MC-ICP-MS. Terr. Atmos. Ocean. Sci. 20, 703–712.

Chen, H.-W., Lee, T., Lee, D.-C., Chen, J.-C., 2015. Correlation of ^{48}Ca, ^{50}Ti, and ^{138}La heterogeneity in the Allende refractory inclusions. Astrophys. J. 806, L21.

Clayton, D.D., 1978. Precondensed matter: key to the early solar system. Moon Planets 19, 109–137.

Connelly, J.N., Bizarro, M., Ivanova, M., Krot, A.N., 2011. Towards a new absolute chronology for the early solar system. Workshop on Formation of the First Solids in the Solar System, #9060.

Davis, A.M., Zhang, J., Hu, J., Greber, N.D., Dauphas, N., 2016. Titanium isotopic anomalies, titanium mass fractionation effects, and rare earth element patterns in Allende CAIs and their relationships. Lunar Planet. Sci XLVII (#3023).

Dodson, M.H., Compston, W., Williams, I.S., Wilson, J.F., 1988. A search for ancient detrital zircons in Zimbabwean sediments. J. Geol. Soc. Lond. 145, 977–983.

Fahey, A.J., Goswami, J.N., McKeegan, K.D., Zinner, E., 1985. Evidence for extreme ^{50}Ti enrichments in primitive meteorites. Astrophys. J. 296, L17–L20.

Fahey, A.J., Goswami, J.N., McKeegan, K.D., Zinner, E., 1987. ^{26}Al, ^{244}Pu, ^{50}Ti, REE, and trace element abundances in hibonite grains from CM and CV meteorites. Geochim. Cosmochim. Acta 51, 329–350.

Fujii, T., Imagawa, J., Nishizawa, K., 1998. Influences of nuclear mass, size shape and spin on chemical isotope effect of titanium. Ber. Bunsenges. Phys. Chem. 102, 1880–1885.

Fujii, T., Moynier, F., Albarede, F., 2006. Nuclear field vs. nucleosynthetic effects as cause of isotopic anomalies in the early solar system. Earth Planet. Sci. Lett. 247, 1–9.

Heydegger, H.R., Foster, J.J., Compton, W., 1982. Terrestrial, meteoritic, and lunar Ti isotopic ratios reevaluated: evidence for correlated variations. Earth Planet. Sci. Lett. 58, 406–418.

Hinton, R.W., Davis, A.M., Scatena-Wachel, D.E., 1987. Large negative ^{50}Ti anomalies in refractory inclusions from the Murchison carbonaceous chodnrite: evidence for incomplete mixing of neutron-rich supernova ejecta into the solar system. Astrophys. J. 313, 420–428.

Huang, S., Farkas, J., Yu, G., Petaev, M.I., Jacobsen, S.B., 2011. Calcium isotopic ratios and rare earth element abundances in refractory inclusions from the Allende CV3 chondrite. Geochim. Cosmochim. Acta 77, 252–265.

Ireland, T.R., 1990. Presolar isotopic and chemical signatures in hibonite-bearing refractory inclusions from the Murchison carbonaceous chondrite. Geochim. Cosmochim. Acta 54, 3219–3237.

Ireland, T.R., Compston, W., Heydegger, H.R., 1985. Titanium isotopic anomalies in hibonites from Murchison carbonaceous chondrite. Geochim. Cosmochim. Acta 49, 1989–1993.

Jacobsen, B., Yin, Q.-Z., Moynier, F., Amelin, Y., Krot, A.N., Nagashima, K., Hutcheon, I.D., Palme, H., 2008. ^{26}Al–^{26}Mg and ^{207}Pb–^{206}Pb systematics of Allende CAIs: canonical solar initial $^{26}Al/^{27}Al$ ratio reinstated. Earth Planet. Sci. Lett. 272, 353–364.

Janney, P.E., Richter, F.M., Mendybaev, R.A., Wadhwa, M., Georg, R.B., Watson, E.B., Hines, R.R., 2011. Matrix effects in the analysis of Mg and Si isotope ratios in natural and synthetic glasses by laser ablation-multicollector ICPMS: a comparison of single- and double-focusing mass spectrometers. Chem. Geol. 281, 26–40.

Jungck, M.H.A., Shimamura, T., Lugmair, G.W., 1984. Ca isotope variations in Allende. Geochim. Cosmochim. Acta 48, 2651–2658.

Lee, T., Papanastassiou, D.A., Wasserburg, G.J., 1978. Calcium isotopic anomalies in the Allende meteorite. Astrophys. J. 220, L21–L25.

Lee, T., Russell, W.A., Wasserburg, G.J., 1979. Calcium isotopic anomalies and the lack of aluminum-26 in an unusual Allende inclusion. Astrophys. J. 228, L93–L98.

Leya, I., Schönbächler, M., Wiechert, U., Krähenbühl, U., Halliday, A.N., 2008. Titanium isotopes and the radial heterogeneity of the solar system. Earth Planet. Sci. Lett. 266, 233–244.

Leya, I., Schönbächler, M., Krähenbühl, U., Halliday, A.N., 2009. New titanium isotope data for Allende and Efremovka CAIs. Astrophys. J. 702, 1118–1126.

Loss, R.D., Lugmair, G.W., Davis, A.M., MacPherson, G.J., 1994. Isotopically distinct reservoirs in the solar nebula: isotope anomalies in Vigarano meteorite inclusions. Astrophys. J. 436, L193–L196.

Lugaro, M., Davis, A.M., Gallino, R., Savina, M.R., Pellin, M.J., 2004. Constraints on AGB models from the heavy-element composition of presolar SiC grains. Mem. Soc. Astron. Ital. 75, 723–728.

Moynier, F., Simon, J.I., Podosek, F.A., Meyer, B.S., Brannon, J., DePaolo, J., 2010. Ca isotope effects in Orgueil leachates and the implications for the carrier phases of 54Cr anomalies. ApJL. 718, L7–L13.

Niederer, F.R., Papanastassiou, D.A., 1984. Ca isotope in refractory inclusions. Geochim. Cosmochim. Acta 48, 1279–1293.

Niederer, F.R., Papanastassiou, D.A., Wasserburg, G.J., 1980. Endemic isotopic anomalies in titanium. Astrophys. J. 240, 73–77.

Niederer, F.R., Papanastassiou, D.A., Wasserburg, G.J., 1981. The isotopic composition of Ti in the Allende and Leoville meteorites. Geochim. Cosmochim. Acta 45, 1017–1031.

Niederer, F.R., Papanastassiou, D.A., Wasserburg, G.J., 1985. Absolute isotopic abundances of Ti in meteorites. Geochim. Cosmochim. Acta 49, 835–851.

Niemeyer, S., Lugmair, G.W., 1981. Ubiquitous isotopic anomalies in Ti from normal Allende inclusions. Earth Planet. Sci. Lett. 53, 211–225.

Niemeyer, S., Lugmair, G.W., 1984. Titanium isotopic anomalies in meteorites. Geochim. Cosmochim. Acta 48, 1401–1416.

Papanastassiou, D.A., Brigham, C.A., 1989. The identification of meteorite inclusions with isotope anomalies. Astrophys. J. 338, L37–L40.

Rauscher, T., Heger, A., Hoffman, R.D., Woosley, S.E., 2002. Nucleosynthesis in massive stars with improved nuclear and stellar physics. Astrophys. J. 576, 323–348.

Russell, S.S., Huss, G.R., Fahey, A.J., Greenwood, R.C., Hutchison, R., Wasserburg, G.J., 1998. An isotopic and petrologic study of calcium–aluminum-rich inclusions from CO3 meteorites. Geochim. Cosmochim. Acta 62, 689–714.

Shaheen, M.E., Gagnon, J.E., Fryer, B.J., 2012. Femtosecond (fs) lasers coupled with modern ICP-MS instruments provide new and improved potential for in situ elemental and isotopic analyses in the geosciences. Chem. Geol. 330-331, 260–273.

Srinivasani, G., Huss, G.R., Wasserburg, G.J., 2000. A petrographic, chemical, and isotopic study of calcium-aluminum-rich inclusions and aluminum-rich chondrules from the Axtell (CV3) chondrite. Meteorit. Planet. Sci. 35, 1333–1354.

Woosley, 1997. Neutron-rich nucleosynthesis in carbon deflagration supernova. Astrophys. J. 476, 801–810.

Trinquier, A., Elliott, T., Coath, C., Krot, A.N., Bizzaro, M., 2009. Origin of nucleosynthetic isotope heterogeneity in the solar protoplanetary disk. Science 324, 374–376.

Vermeesch, P., 2004. How many grains are needed for a provenance study? Earth Planet. Sci. Lett. 224, 441–451.

Wasserburg, G.J., Lee, T., Papanastassiou, D.A., 1977. Correlated O and Mg isotopic anomalies in Allende inclusions: II. Magnesium. Geophys. Res. Lett. 4, 299–302.

Weber, D., Zinner, E., Bischoff, A., 1995. Trace element abundances and magnesium, calcium, and titanium isotopic compositions of grossite-containing inclusions from the carbonaceous chondrite Acfer 182. Geochim. Cosmochim. Acta 59, 803–823.

Williams, C.D., Wadhwa, M., Janney, P.E., Hines, R.R., Bullock, E.M., MacPherson, G.J., 2012. Ti, Si and Mg isotope systematics of FUN CAI CMS-1. Meteoritical Society Meeting #5102.

Williams, C.D., Ushikubo, T., MacPherson, G.J., Bullock, E.M., Kita, N.T., Wadhwa, M., 2013. Oxygen isotope systematics of Allende FUN CAI CMS-1. Lunar Planet. Sci. XLIII (#2435).

Zhang, J., Dauphas, N., Davis, A.M., Pourmand, A., 2011. A new method for MC-ICPMS measurement of titanium isotopic composition: identification of correlated anomalies in meteorites. J. Anal. At. Spectrom. 26, 2197.

Zhang, J., Dauphas, N., Davis, A.M., Leya, I., Fedkin, A., 2012. The proto-Earth as a significant source of lunar material. Nat. Geosci. 5, 251–255.

Zinner, E.K., Fahey, A.J., Goswami, J.N., Ireland, T.R., McKeegan, K.D., 1986. Large ^{48}Ca anomalies are associated with ^{50}Ti anomalies in Murchison and Murray hibonites. Astrophys. J. 311, L103–L107.